Marine Chemistry 168 (2015) 140–150

Contents lists available at ScienceDirect

Marine Chemistry

journal homepage: www.elsevier.com/locate/marchem

Upwelling velocity and eddy diffusivity from ^{7}Be measurements used to compare vertical nutrient flux to export POC flux in the Eastern Tropical South Pacific

William Z. Haskell II [a,*], David Kadko [b], Douglas E. Hammond [a], Angela N. Knapp [c], Maria G. Prokopenko [a], William M. Berelson [a], Douglas G. Capone [d]

[a] Dept. of Earth Sciences, University of Southern California, 3651 Trousdale Pkwy, Los Angeles, CA, 90089, United States
[b] RSMAS, University of Miami, 4600 Rickenbacker Causeway, Miami, FL 33149, United States
[c] Earth, Ocean and Atmospheric Science Dept., Florida State University, Tallahassee, FL 32306, United States
[d] Dept. of Biological Sciences, University of Southern California, 3616 Trousdale Pkwy, Los Angeles, CA 90089, United States

ARTICLE INFO

Article history:
Received 2 June 2014
Received in revised form 1 October 2014
Accepted 1 October 2014
Available online 22 October 2014

Keywords:
Upwelling
Eddy diffusivity
New production
Export
Nutrient cycling

ABSTRACT

Five ^{7}Be profiles, measured in an area bounded by 10°S–20°S and 80°W–100°W, were used to determine upwelling velocity (w_H) and vertical diffusivity (K_z). A positive correlation between w_H and ^{14}C primary production rate and a negative correlation between the inventories of ^{7}Be and phosphate were observed. We interpret this as the influence of deeper, nutrient-rich, ^{7}Be-poor water brought up by upwelling. Excluding two stations that appear to be influenced by non-steady state dynamics or horizontal transport, upwelling velocities were estimated to be 0 to 1.0 m d^{-1} and K_z values ranged from 0.4 to 2.6 cm^2 s^{-1}. From these parameters, NO_3^- fluxes into the euphotic zone were assessed and ranged from 0.15 to 2.9 mmol m^{-2} d^{-1}. Using these values, we estimate 1.0 to 19 mmol C m^{-2} d^{-1} of new production in the ETSP. New production based on ^{7}Be-derived transport parameters agree with carbon export estimates using a ^{234}Th balance, sediment traps and O_2/Ar supersaturation for stations along 20°S, but are higher than export estimates at 10°S, 100°W.

1. Introduction

The vertical transport of nutrients in the upper ocean is vital to biogeochemical cycling and the ocean's ability to sequester atmospheric carbon dioxide via the supply of particulate organic carbon to deep-sea ecosystems. The uncertainty involved in estimating eddy diffusivity, an important mechanism for transporting subsurface nutrients into surface waters, is substantial, and direct measurement of upwelling velocity is difficult, in part because of the small velocities involved. Previously employed approaches typically utilize surface anomalies in tracers found in thermocline waters, including ^{14}C, δ^{13}C, Apparent Oxygen Utilization (AOU), δ^{3}He, pCO_2, and temperature (Broecker and Peng, 1982; Broecker et al., 1978; Klein and Rhein, 2004; Quay et al., 1983; Rhein et al., 2010; Wanninkhof et al., 1995). Uncertainties in gas exchange, primary production, and the air-sea equilibration rate of CO_2 (~1 yr) limit the effectiveness of many of these tracers. In order to determine local and time-dependent upwelling velocities, a tracer with a timescale of weeks is desirable. While the tritiugenic ^{3}He-based approach does integrate over the time scale of gas exchange in the mixed layer, accurate knowledge of the gas exchange velocity and vertical diffusivity at the base of the mixed layer must be known to effectively utilize this method for estimating upwelling velocity.

^{7}Be (half-life: 53 d) is a cosmic-ray produced radionuclide deposited on the ocean surface mainly by rainfall and reaches a uniform activity within the mixed layer (Aaboe et al., 1981; Kadko, 2000, 2009; Kadko and Olson, 1996; Silker, 1972a,b; Young and Silker, 1980). It has been demonstrated that ^{7}Be is quite soluble in the relatively low particle density environments of the open ocean (<10% loss to particle adsorption; Silker, 1972; Aaboe et al., 1981; Andrews et al., 2008; Kadko and Prospero, 2011; Kadko and Johns, 2011). Therefore, if radioactive decay is the only removal process, then the inventory in the water column is equal to the integrated input flux over approximately the mean life of the isotope (~77 d). Previous studies have used the penetration of ^{7}Be-rich mixed layer water to trace subduction and ventilation of the upper thermocline over a seasonal timescale and to estimate mixing rates (Kadko, 2000; Kadko and Johnson, 2008; Kadko and Olson, 1996; Kadko and Swart, 2004). In this study, we used ^{7}Be to evaluate upwelling, following the approach of Kadko and Johns (2011) in the Equatorial Atlantic: The dilution of the ^{7}Be-rich mixed layer by ^{7}Be-depleted waters from below is used to estimate upwelling velocities by mass balance calculations. Furthermore, with knowledge of upwelling rates, vertical eddy diffusivities may then be calculated from ^{7}Be profiles. This technique was used during a cruise to the Eastern

* Corresponding author. Tel.: +1 240 687 0772; fax: +1 213 740 8801.
E-mail address: whaskell@usc.edu (W.Z. Haskell).

http://dx.doi.org/10.1016/j.marchem.2014.10.004
0304-4203/

Tropical South Pacific (ETSP) from March 23 to April 28, 2011 to investigate surface ocean nutrient budgets, in order to complement a larger effort of characterizing the nitrogen cycle surrounding the intense Oxygen Minimum Zone (OMZ) found in this region.

2. Methods

2.1. Beryllium-7

Five stations were sampled for ^{7}Be at three depths between 10°S–20°S and 80°W–100°W (Fig. 1). Sampling depths were chosen based on the strength of the temperature gradient observed during CTD descent, which should reflect the extent of vertical mixing, and thus the depth of ^{7}Be penetration into the water column. Samples from the mixed layer (200 L), about 20 m below the mixed layer (400 L), and about 20 m below that (600 L), were taken with a CTD equipped with twelve, 30 L Niskin bottles, on multiple casts. Water from each depth was transferred into 208 L drums via 10 L buckets, and then pumped twice through a cartridge containing FeOH-impregnated acrylic fibers for ^{7}Be extraction (Krishnaswami et al., 1972; Lal et al., 1988; Lee et al., 1991). The efficiency of the fiber for extraction of ^{7}Be from seawater has previously been determined by adding a stable Be atomic absorption standard to a drum containing seawater. As described in Kadko and Johns (2011), seawater was pumped through an iron fiber cartridge and at every 100 L the Be content of the cartridge effluent was measured by atomic absorption. From this data, the integrated Be extraction efficiencies were calculated. For sample volumes in the range 400–700 L, based on several trials, the extraction efficiencies were respectively, 82 ± 3% to 76 ± 2%. In this study, the drums and buckets used for transfer from the CTD were rinsed thoroughly with fresh water prior to processing each sample. Fibers were then removed from the cartridges and placed into bags for transport to the University of Miami, where they were subsequently dried, ashed, pressed into 5.8 cm diameter 'pucks' and counted on an Ortec low-background, High Purity Germanium (HPGe) gamma detector. The analysis is described in detail elsewhere (Kadko, 2009). ^{7}Be has a readily identifiable gamma peak at 478 keV. The detector was calibrated for puck geometry by adding a commercially prepared solution of known mono-energetic gamma activities (thus avoiding summation corrections) to an ashed fiber; these were treated identically to a sample. From these data, a calibration curve based on puck thickness (in the range 7–13 mm) was derived. The uncertainty of extraction efficiency (4%) and the detector efficiency (2%) was in all cases smaller than the statistical counting error and the uncertainty in the blank.

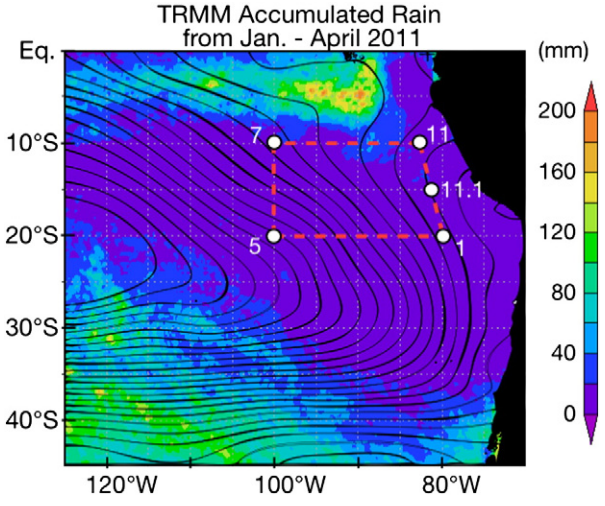

Fig. 1. ETSP cruise track and rainfall estimates. Map of the cruise track (red dashed lines) showing the location of each station sampled for ^{7}Be (Stations shown with white circles and numbered) overlaid on TRMM accumulated rainfall estimates from January to April, 2011 over the study region (colors; NASA, 2014). Black lines are spring dynamic height isopleths relative to 1000 m acquired from World Ocean Atlas 2009 (Schlitzer, 2014; World Ocean Atlas, 2009).

2.2. Nutrients

Nutrients were collected from 24 depths at each station via a CTD equipped with 24 10 L Niskin bottles. Samples collected in the upper 400 m were filtered through a 0.2 μm syringe filter before collection in acid-washed 60 mL HDPE Nalgene bottles that were rinsed with sample water three times before filling. The concentration of nitrate plus nitrite ($NO_3^- + NO_2^-$) was determined on samples frozen at −20 °C at sea and analyzed on land using the chemiluminescent method of Braman and Hendrix (1989) in a configuration with a detection limit of ~0.05 μM. The average standard deviation for replicate [$NO_3^- + NO_2^-$] analysis from an individual sample was ±0.1 μM. The concentrations of NO_2^- and phosphate (PO_4^{3-}) were measured at sea using colorimetric methods described by Strickland and Parsons (1968) with a detection limit of 50 nM and standard deviation of ±20 nM for both NO_2^- and PO_4^{3-} analyses. Measurements of dissolved silica were made on refrigerated samples transported back to USC and analyzed colorimetrically with a Hitachi UV/vis-spectrophotometer at 810 nm (Parsons et al., 1984).

2.3. Floating sediment traps

Two strings of floating Particle Interceptor Sediment Traps (PITs) were deployed at both 100 m and 200 m for an average of ~35 h at Stations 1, 11, 11.1, and for ~65 h at Stations 5 and 7. All traps had 12 collection tubes with an aspect ratio of 6.4 and 5 cm thick baffles (1 cm × 1 cm) fitted into the top opening of the tubes. Funnels with centrifuge tubes (Falcon, 50 mL) were attached into the base of each trap tube. Each centrifuge tube contained a brine solution of NaCl and $NaBO_4$ (in excess of sea water by 5 ppt) poisoned with 2% Formaldehyde. After retrieval, swimmers were picked from each trap sample under a microscope, the remaining material was combined onto two Whatman GF/F (0.7 μm poresize) filters and one Whatman polycarbonate membrane filter (0.4 μm), and then each was weighed. One GF/F filter was used for gamma spectroscopy at USC, the polycarbonate membrane filter was used for bSi analysis at USC, and the other GF/F was sent to UC Davis Stable Isotope Facility (SIF) for C and N analysis. The measured values were then scaled up by mass to the entire trap catch. A detailed description of this method can be found in Haskell et al. (2013).

2.4. Thorium-234

Ten depths from the surface to 300 m were chosen based on fluorescence measured with a SeaBird sensor during the CTD's descent. An isotope dilution method using a ^{229}Th spike of known activity and coprecipitation with MnO_2 was used to measure ^{234}Th (Rutgers van der Loeff and Moore, 1999). The ^{234}Th deficit relative to its parent isotope, ^{238}U, was calculated by trapezoidal integration of the profile. The POC:^{234}Th and bSi:^{234}Th ratios measured in trap material were used to estimate organic carbon and bSi fluxes on sinking particles. A detailed description of these calculations can be found in Haskell et al. (2013).

3. Results and discussion

3.1. Box model

To investigate the vertical transport of nutrients and tracers in the upper thermocline, we used a simple, one-dimensional box model of the upper ocean consisting of a surface mixed layer of uniform concentration underlain by a gradient with depth, adopting the convention that depth (z) is positive downward. We assume that upwelled water

enters the mixed layer from below and exits horizontally. The change in concentration (C) of any nutrient or tracer over time (per m^2) in a mixed layer of depth H should be given by:

$$H\frac{\partial C}{\partial t} = F_a - J - \lambda C_o H + w_H C_o - P \tag{1a}$$

where

$$J = w_H C_H - K_z\left(\frac{\partial C}{\partial z}\right)_H \tag{1b}$$

Terms include input from production (F_a), flux from below due to upwelling and eddy diffusivity (J, where C_H is the concentration in upwelled waters, K_z is the eddy diffusivity, and $\partial C/\partial z$ is the concentration gradient with depth), decay within the surface box ($\lambda C_o H$; where λ is the decay constant if the tracer is radioactive, C_o is the mixed layer concentration), loss to particle export (P), and loss from horizontal export ($w_H C_o$; where w_H is the upwelling velocity at depth H). Because depth is taken as positive downward ($z \geq 0$), upwelling into the mixed layer is negative ($w_H \leq 0$). Note that if the surface layer is a constant thickness, the effective horizontal export at the surface must have the same velocity as upwelling, but the term has the opposite sign. The change in concentration below the mixed layer box over time, assuming constant upwelling velocity below the mixed layer (w) and K_z, is given by:

$$\frac{\partial C}{\partial t} = \frac{\partial}{\partial z}K_z\left(\frac{\partial C}{\partial z}\right) - \lambda C - w\frac{\partial C}{\partial z}. \tag{2}$$

3.2. Estimated upwelling rates and eddy diffusivity

To estimate upwelling velocity from ^{7}Be, we used a steady state formulation of the one-dimensional box model (combining Eqs. 1a and 1b), neglecting particle export (Section 3.6), to formulate a mass balance. The model includes a mixed layer with uniform ^{7}Be activity (C_o) (Eq. 3) and an underlying layer where the ^{7}Be activity (C_z) decays exponentially with depth (Fig. 2).

$$0 = F_a + K_z\left(\frac{\partial C}{\partial z}\right)_H - \lambda C_o H + w_H(C_o - C_H). \tag{3}$$

In this case, F_a is the atmospheric ^{7}Be input flux to the mixed layer, λ is the ^{7}Be decay constant and the mixed layer depth is defined as the depth where the temperature changes from its surface value by 0.5 °C (Hayes et al., 1991). Previous studies have shown that ^{7}Be decreases exponentially with depth below the mixed layer (Andrews et al., 2008; Kadko, 2009; Silker, 1972a, b). Following the approach of Kadko and Johns (2011), the ^{7}Be activity below the mixed layer is determined to a first approximation by the one-dimensional vertical advection–diffusion equation and the decay of ^{7}Be in Eq. 2. Assuming steady state, constant w, constant K_z, and $C(z) = C_o$ through the mixed layer to depth H, the solution to Eq. 2 is a simple exponential:

$$C(z) = C_o e^{-\alpha(z-H)} \tag{4}$$

where the depth attenuation coefficient (α) is given by:

$$\alpha = \frac{-w}{2K_z} + \frac{1}{2}\left\{\left(\frac{w}{K_z}\right)^2 + \left(\frac{4\lambda}{K_z}\right)\right\}^{1/2}. \tag{5}$$

The input flux of ^{7}Be by atmospheric fallout (F_a) is dominated by wet deposition (>80%; Reiter, 1978; Kadko and Prospero, 2011). The colormap in Fig. 1 is a map view of monthly accumulated rainfall, measured by NASA's Tropical Rainfall Measuring Mission (TRMM), from three months prior to the beginning of the cruise, through the end of the cruise in April 2011 (NASA, 2014). Although the average rainfall in this region is small (~1 cm $month^{-1}$), it appears to be uniform and we assume the input flux is consistent throughout the study area. We also assume the station closest to the central gyre (Station 5) has an upwelling velocity of zero. This makes Station 5 our 'standard' station against which ^{7}Be inventories are compared. The inventories of ^{7}Be were calculated using the 3 samples obtained at each station (Table 1; Table 2). The difference in the ^{7}Be inventory at each station relative to the station with no upwelling (Station 5) provides an estimate of upwelling rates (Kadko and Johns, 2011; Kadko and Prospero, 2011). Eqs. 3 and 4 can be modified to relate upwelling velocity at the base of the mixed layer (w_H) to the water column ^{7}Be inventory (C_{inv}; dpm m^{-2}) by first integrating Eq. 2 below the mixed layer, noting that the activity of ^{7}Be approaches zero at depth:

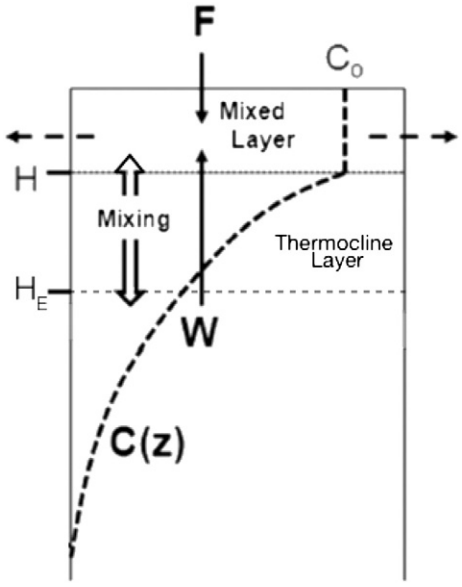

Fig. 2. Upper thermocline box model. Box model used in upwelling calculation (adapted from Kadko and Johns, 2011). C_o = activity of ^{7}Be in the mixed layer (dpm 1000 L^{-1}), w = upwelling velocity in the upper thermocline (m d^{-1}), H = mixed layer depth (m), and H_E = depth of euphotic zone. In this study, we chose 10 m below the deep Chl-a maximum (DCM) to represent this depth (Section 3.4). The dashed line is the profile of the ^{7}Be activity in the upper thermocline. The dashed arrows represent horizontal flow.

$$0 = K_z\left(\frac{\partial C}{\partial z}\right)_H - \lambda\int_H^\infty C(z)dz + w_H C_H - \int_H^\infty C(z)\frac{\partial w}{\partial z}sz. \tag{6}$$

After combining Eq. 6 with Eq. 3 and canceling terms, an equation for the total water column ^{7}Be balance is given:

$$-w_H C_o = F_a - \lambda C_{inv} + \int_H^\infty C(z)\frac{\partial w}{\partial z}dz \tag{7a}$$

where

$$C_{inv} = \int_0^\infty C(z)dz = C_o H + \frac{1}{\alpha}C_o. \tag{7b}$$

The last term in Eq. 7a represents any depth-dependent changes in w below the mixed layer. If the vertical velocity below the mixed layer is constant, Eq. 7a becomes:

$$-w_H = \frac{1}{C_o}(F_a - \lambda C_{inv}) \tag{8}$$

Table 1
^{7}Be water column data.

Station	Lat./long.	Date	Depth (m)	^{7}Be (dpm m^{-3})	MLD[a] (m)	ML temp[b] (°C)	ML [PO_4][c] (uM)	ML [NO_3] (uM)	ML Si (uM)
1	20° S 80° W	3/26/11	25	306 ± 26	40	22.13	0.38	0.06	0.13
			55	58 ± 13					
			80	43 ± 12					
5	20° S 100° W	4/10/11	40	299 ± 26	60	23.35	0.33	0.03	0.36
			70	154 ± 8					
			83	86 ± 14					
7	10° S 100° W	4/5/11	20	164 ± 25	40	26.18	0.67	7.3	2.5
			55	54 ± 14					
			68	51 ± 9					
11	10° S 82° W	3/30/11	15	86 ± 24	32	25.17	0.57	3.8	1.35
			40	27 ± 20					
			70	97 ± 8					
11.1	15° S 81° W	4/18/11	20	243 ± 19	27	22.75	0.57	0.46	0.68
			51	84 ± 10					
			73	115 ± 8					

[a] Mixed layer depth.
[b] Mixed layer temperature.
[c] [PO_4] and [NO_3] from Knapp et al., in prep.

where upwelling is negligible, Eq. 7a becomes:

$$F_a = \lambda C_{inv} \quad (9)$$

which represents the balance between atmospheric flux of ^{7}Be to the ocean and radioactive decay. Note that in the previous equations, if water is upwelling, w_H is negative because our depth (z) is taken as positive downward. In the subsequent discussion, we will refer to 'upwelling,' indicating $w_H < 0$ as water entering the surface box from below.

In this study, the calculated upwelling rates from Eq. 8, here after referred to as 'Method A,' ranged from 0.0 to 2.95 m d^{-1} (Table 2 column 'A'), which is comparable to other estimates from this region (1.4–1.7 m d^{-1}; Wyrtki, 1963; Toggweiler et al., 1991). However, at two stations (11 and 11.1), the deepest sample is inconsistent with the 1-D model and has been ignored. Consequently, these inventories should be considered as lower limits and values for w_H and K_z are upper limits, including the highest upwelling velocity of 2.95 m d^{-1}. The cause of the vertical distribution of ^{7}Be at these stations is unknown, but possible contributing factors are discussed in Section 3.6. Neglecting Stations 11 and 11.1, the range of upwelling velocities observed was 0–1.1 m d^{-1}, with an average of 0.5 m d^{-1}.

A plot of the calculated upwelling velocities versus integrated ^{14}C primary production (Capone et al., in prep) throughout the euphotic zone is shown in Fig. 3, which displayed a positive correlation. This relationship is expected if primary production is fueled by upwelled nutrients in the euphotic zone. A negative correlation between water column ^{7}Be inventories and integrated phosphate concentration to 100 m was also observed (Fig. 3). We interpret this relationship as the upwelling of deep ^{7}Be-depleted, nutrient-rich water into the upper thermocline and mixed layer in a region which is not limited by phosphate. Since it is not limiting production, phosphate accumulates in the upper 100 m because it is introduced at a higher rate than it is consumed by phytoplankton.

As described in Kadko and Johns (2011), uncertainties in upwelling estimates due to the neglect of horizontal advection of ^{7}Be from regions of higher concentration can be estimated by examining the horizontal gradients in mixed layer ^{7}Be concentration and magnitudes of horizontal surface velocities ($H * (u_o \partial C_o / \partial x + v_o \partial C_o / \partial y)$), and then comparing this term to the size of the atmospheric flux (F_a = 299 dpm m^{-2} d^{-1}). At the stations farthest west, closest to the SPG (Stations 5 and 7), surface currents averaged about 5 cm s^{-1} throughout the austral fall (NOAA, 2011) and the zonal surface ^{7}Be gradient between the two stations was about 0.12 dpm m^{-3} km^{-1}. This would lead to an uncertainty in w_H of approximately 5.5%. Along the eastern boundary of the cruise track, where the surface ^{7}Be gradients were between 0.11 and 0.28 dpm m^{-3} km^{-1}, the surface currents average around 10 cm s^{-1} and thus the uncertainty in w_H due to horizontal advection may be on the order of 5–10%. The uncertainties in w_H reported in Table 2 are the sum of the uncertainties from horizontal advection and the curve fitting to find the water column ^{7}Be inventory. The estimates

Table 2
^{7}Be inventories, box model calculations, and eddy diffusivities.

Station	MLD[a] (m)	C_o[b] (dpm m^{-3})	C_{inv}[c] (dpm m^{-2})	α[d] (m^{-1})	σ	A w_H[e] (m d^{-1})	σ	A K_z[f] (cm^2 s^{-1})	σ	B w_H (m d^{-1})	σ	B K_z (cm^2 s^{-1})	σ
1	40	306	15,239	0.102	±0.04	0.33	±0.06	0.52	±0.22	0.17	±0.04	0.34	±0.13
5	60	299	22,993	0.059	±0.03	0.00	±0.08	0.43	±0.23	−0.16	±0.04	0.11	±0.013
7	40	164	9302	0.059	±0.03	1.09	±0.20	2.56	±1.46	0.79	±0.12	1.97	±0.69
11	32	86	3365	0.144	±0.10	2.95	±0.91	2.45	±1.85	2.39	±0.46	1.99	±0.59
11.1	27	243	12,086	0.044	±0.02	0.58	±0.12	2.30	±1.29	0.38	±0.07	1.78	±0.44

Method A — assuming upwelling of 0 m d^{-1} at Sta. 5.
Method B — assuming the atmospheric flux of ^{7}Be is 250 dpm m^{-2} d^{-1} (Nagai et al., 2000).
[a] Mixed layer depth.
[b] Mixed layer ^{7}Be activity.
[c] ^{7}Be inventory.
[d] Depth attenuation coefficient. Uncertainty calculated from propagating counting uncertainty and the uncertainty in the curve fit.
[e] Upwelling velocity. Uncertainty calculated from the standard deviation of the ^{7}Be inventory caused by uncertainty in α and uncertainty introduced from horizontal transport (Section 3.2).
[f] Eddy diffusivity in the upper thermocline. Uncertainty calculated from propagating the uncertainty in w_H and α.

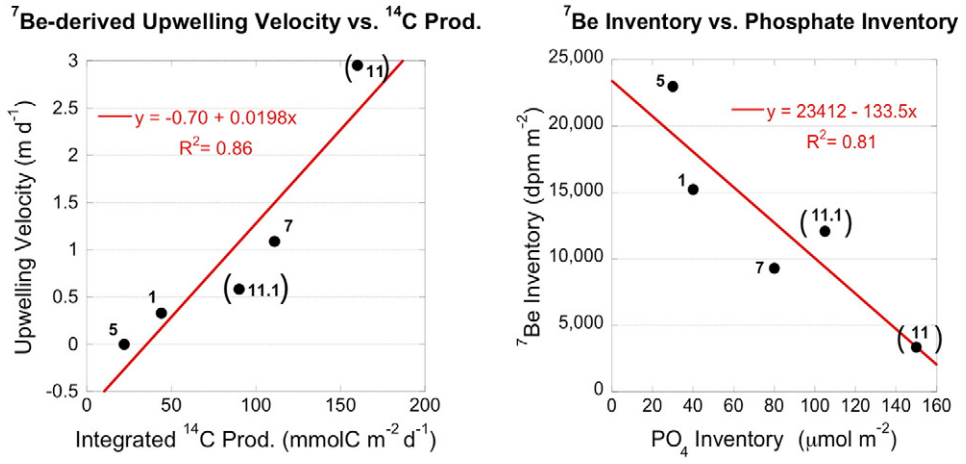

Fig. 3. ^{7}Be data plotted versus phosphate and ^{14}C production. Left: Upwelling velocities calculated from the ^{7}Be mass balance at each station plotted against ^{14}C primary productivity integrated to the 1% light horizon. Right: ^{7}Be inventories in the water column at each station plotted against the inventory of phosphate in the upper 100 m. Data from Stations 11 and 11.1 are presented in parenthesis because upwelling velocity at these sites are most likely over estimates (see text). Solid lines are linear regressions of all five points in each plot.

of upwelling rate determined by Eq. 5 may be a lower limit because we assume the upwelling velocity is constant below the mixed layer. If the upwelling velocity is not constant, but instead decreases with depth (Harrison, 1996; Quay et al., 1983) due to lateral convergence within the upper thermocline (Wyrtki, 1981; Fig. 2), it is possible that the actual w_H could be higher. Kadko and Johns (2011) tested whether w(z) structure influences the model results and found that the estimates assuming a constant w provide upwelling rates within 8 ± 12% of those which assume w decreases linearly with depth below the mixed layer. We assume here that the uncertainty of about 10% in upwelling velocity, introduced by assuming constant w, is minor compared to other factors. A more detailed derivation of this model, its uncertainties, as well as an assessment of its applicability, can be found in Kadko and Johns (2011).

We would like to clarify that upwelling is most likely non-uniform in space throughout our study area and that the upwelling velocity at each station most likely reflects the vertical transport signal within ~5° of the sampling site. Over its mean lifetime of ~80 days, at the mean observed current velocity of ~5–10 cm s^{-1}, ^{7}Be can travel ~3–7°. Nonetheless, we can test whether our calculated upwelling velocities are on the right order of magnitude by using a simple 2-dimensional calculation, which balances the total vertical and horizontal fluxes throughout the study area. The mean upwelling rate (w_H) times the width of the surface box across our study region (L) should equal the mean surface layer depth (H) times the mean horizontal flow rate (v_x; $w_H * L = H * v_x$). The average upwelling velocity is ~0.5 m d^{-1} and the length of the path of mean streamlines across our study area is ~10° (1000 km), given that the direction of flow is to the northwest (Fig. 1). Assuming the mean surface layer depth is ~50 m, the horizontal flow rate of upwelling water in our study region should rise from 0 to 10 cm s^{-1}, comparable to what was observed in the ETSP during this study. This balance neglects the third dimension of horizontal flow, thus the true horizontal velocity due to upwelling is most likely less than 10 cm s^{-1}.

3.2.1. Eddy diffusivity

Vertical mixing by eddy diffusivity is not considered in the mass balance used to determine upwelling velocity because it does not influence the ^{7}Be inventory (Fig. 2), but it does influence the shape of the ^{7}Be profile and the mixed layer concentration. The shape is dictated by the balance between upwelling of ^{7}Be-deficient water into the mixed layer and downward turbulent mixing of ^{7}Be-rich water from the surface layer (Kadko and Johns, 2011). The portion of the ^{7}Be inventory contained below the mixed layer gives insight into the strength of local vertical eddy diffusive mixing. In the case of weak vertical mixing and/or strong upwelling, most of the ^{7}Be inventory will be contained within the mixed layer. Conversely, strong vertical mixing and/or relatively low upwelling would deepen ^{7}Be penetration and a large portion of the inventory would be below the mixed layer.

Eq. 4 was fitted to each profile (Fig. 4), with reasonably good results at 3 stations. Using the fitted value of α and the value calculated for w_H using the water column inventory (Eq. 8), Eq. 5 can be used to solve for K_z (Table 2 column 'A'). Diffusivities ranged from 0.43 cm^2 s^{-1} to 2.6 cm^2 s^{-1}. We note a general latitudinal trend of w_H and K_z values in this study with lower values for both along the 20°S transect, and higher values along 10°S, which coincides with the trend in surface concentrations of phosphate and nitrate (Table 1; Knapp et al., in prep). The K_z values obtained in this model are consistent with previous studies in the eastern and central Pacific which employed diffusive gradient models and photosynthetic nitrogen demands to calculate K_z values in the range: 0.5–5.1 cm^2 s^{-1} (Anderson, 1978; Karl et al., 1992; Platt et al., 1984). In a study along the same cruise track one year prior to this study, Yeung et al. (in review) reported K_z values of 0.1 to 1.0 cm^2 s^{-1}, determined using water column ^{222}Rn ($t_{1/2}$ = 3.8 d) profile modeling. Although these values fall below the values reported in this study, we believe the agreement is quite good given the uncertainties in each method, the difference in depths considered and mean lifetime of the isotopes.

Station 5, located at 20°S, 100°W, is the farthest station from the coast and is on the edge of the oligotrophic South Pacific Gyre (SPG). While the assumption that there is no upwelling at Station 5 is reasonable given its proximity to the central gyre, previous studies suggest there may be downwelling at this location (Toggweiler et al., 1991). Modeling efforts using the P2A ocean general circulation model (GCM) have also predicted that in the southern hemisphere central gyre downwelling may be most intense on the eastern side of the central gyre (Gnanadesikan et al., 2004). If this is the case, then the ^{7}Be inventory at Station 5 could be inflated due to convergence of surface waters and downwelling, leading to an over-estimate of the local flux of ^{7}Be from the atmosphere. Another estimate of atmospheric ^{7}Be flux can be made using a value for tropospheric ^{7}Be production based on the neutron and proton cross-sections for ^{14} N at 20°S. Nagai et al. (2000) report a ^{7}Be production rate of 250 dpm m^{-2} d^{-1}, as compared to our value of 299 dpm m^{-2} d^{-1}. It is important to note that the value taken from Nagai et al. (2000) does not necessarily imply that our calculated ^{7}Be input value is an overestimate, because among other things, there are model uncertainties in ^{7}Be production in the atmosphere, and possible non-uniform delivery to the ocean. Its production is dependent on cosmic ray flux, which is heavily influenced by the geomagnetic field and changes in solar magnetic activity. Tropospheric dynamics, stratosphere–troposphere exchange and precipitation also fluctuate in

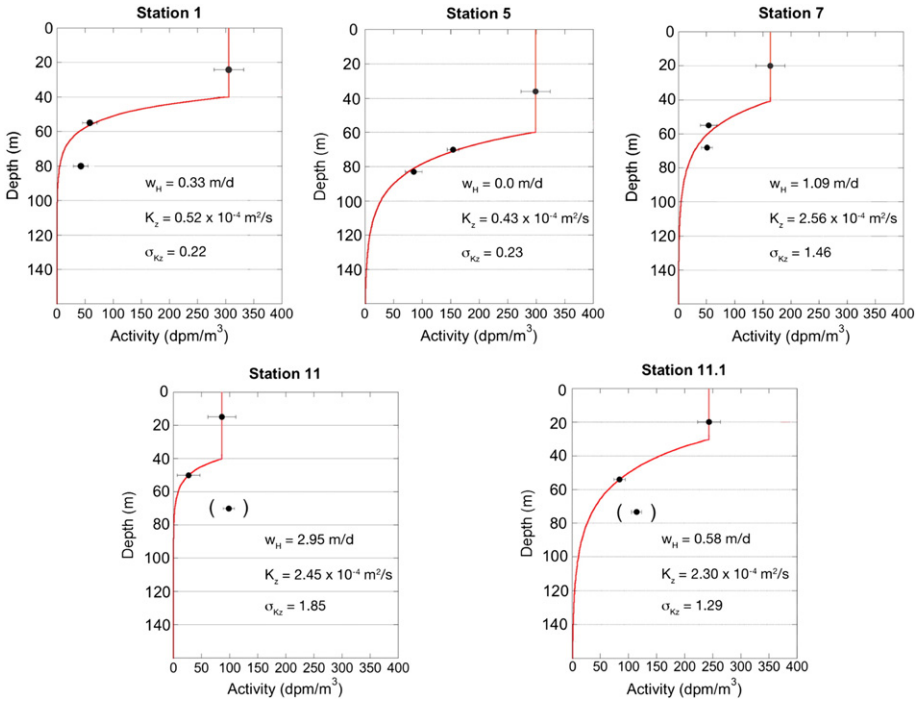

Fig. 4. ^{7}Be profiles measured at each station and fit to an exponential beneath the mixed layer. ^{7}Be profiles fit to an exponential below the base of the mixed layer to obtain eddy diffusivity estimates. The red line shows constant ^{7}Be activity in the mixed layer, according to the assumption made in the box model. Shown on each plot are upwelling velocity (w_H), eddy diffusivity (K_z) and uncertainty in K_z (σ_{Kz}). Uncertainties were propagated from the uncertainty in w_H and the depth attenuation coefficient (α) from the fit. Points in parenthesis were not used for the fit.

space and time (Aldahan et al., 2001; Feely et al., 1989; Forbush, 1954; Leppänen et al., 2010; Vainio et al., 2009). However, taking the Nagai et al., (2000) estimate as the input, defined here as 'Method B,' upwelling velocities and eddy diffusivities both shifted down, ranging from −0.16 to 0.8 m d^{-1}, and 0.11 to 2.0 cm^2 s^{-1}, respectively (Table 2 column 'B').

3.3. Estimating K_z from temperature profiles

Temperature profiles offer an alternative tracer for evaluating vertical diffusivity, assuming that horizontal transport is negligible. A one-dimensional equation for the effect of advection, diffusion, and solar heating was formulated and solved at steady state. As for ^{7}Be, advection and eddy diffusivity were assumed to be constant. The heating function decreased exponentially and was constrained by the solar insolation at these latitudes and the depth attenuation for light. The resulting equation was fit to the temperature profile at each station, through the depth range near the base of the euphotic zone where the nutrient gradient became detectable. The fit provided a measure of w_H/K_z, and the upwelling velocity derived from ^{7}Be was used to calculate K_z. This calculation was quite insensitive to the inclusion of the solar heating term, as light levels were low in the depth range used for fitting.

Table 3
Alpha, w_H, and K_z calculated from temperature profiles.

Station	α_T[a] (m^{-1})	w_H[b] (m d^{-1})	Depth range[c] (m)	K_z[d] (cm^2 s^{-1})
1	0.028	0.33	70–100	1.4
5	0.034	0.00	90–130	–
7	0.013	1.09	90–130	9.6
11	0.015	2.95	90–140	23
11.1	0.019	0.58	100–130	3.6

[a] Depth attenuation coefficient from fit of temperature profiles.
[b] Upwelling velocity from ^{7}Be.
[c] Depth range of temperature profile fit to find α.
[d] Eddy diffusivity calculated from ^{7}Be upwelling velocity and α_T. ($K = w_H\,\alpha^{-1}$).

Table 3 shows the depth attenuation coefficients (α_T) calculated from fitting the temperature profiles at each station and the corresponding calculated eddy diffusivities. Vertical diffusivities were 2 to 9 times larger than those based on fits to the ^{7}Be profiles. One potential reason for the discrepancy is that the response times of temperature and ^{7}Be profiles to perturbations in mixing, or to horizontal transport, are likely to differ. A maximum estimate of the time scale for response to non-steady state events can be made by considering the ratio of the depth range divided by upwelling velocity, which is on the order of 10 to 50 days (excluding Station 5). Because ^{7}Be is also lost by radioactive decay, while solar heating in these depths has minimal impact, the ^{7}Be profiles have a shorter time constant for response to perturbations or horizontal effects, and should provide a better estimate of recent local mixing. A further complication may be introduced if w decreases with depth, as a deeper depth range was chosen for T than for ^{7}Be. As shown below, ^{7}Be estimates of nutrient flux are more compatible with independent production estimates. We believe the diffusivities calculated from heat budgets are too large.

An alternative approach was explored, allowing ^{7}Be input to vary spatially and using fits to temperature and ^{7}Be below the mixed layer to constrain both w and K_z. This approach provides lower estimates of K_z and w at Stations 1, 5 and 7 by factors of 1.5 to 7 and by factors of 4 and 37 at the problematic Stations 11.1 and 11, respectively. However, results of this approach would require the highest ^{7}Be input at Station 5, with decreasing input to the north and east, which does not correspond to rainfall patterns. It would also weaken the correlation of Fig. 3a; we consider it a less likely scenario.

3.4. Nutrient fluxes

In steady-state, new production, defined as primary production fueled by NO_3^- introduced from outside of the euphotic zone or by N_2 fixation, equals the amount of primary production which is available

for export out of a given system (Dugdale and Goering, 1967). The vertical transport of nutrients into the euphotic zone in the open ocean is governed by upwelling and eddy diffusion within the water column. With measured nutrient profiles, as well as both the upwelling velocities and eddy diffusivities calculated above, the vertical transport of inorganic nutrients in the upper thermocline can be assessed. Profiles of potential density, nitrate concentration, and silicic acid concentration are presented in Fig. 5. Following Eq. 1b, the vertical flux from advection (J_{adv}; mmol m^{-2} d^{-1}) of nutrient 'N', can be calculated using upwelling velocity (m d^{-1}) as follows:

$$J_{adv} = w_H * C_N \tag{10}$$

where C_N equals the concentration of 'N'(mmol m^{-3}) in the water upwelled into the euphotic zone. In this study, C_N was chosen as the concentration 10 m below the deep Chlorophyll-a maximum (DCM), determined using a Seabird fluorometer on the CTD's decent. While this choice of depth is admittedly arbitrary (Kadko and Johns, 2011; Swenson and Hansen, 1999), we believe this is an adequate horizon to represent the base of the euphotic zone because there is isotopic evidence of NO_3^- assimilation above this depth in $\delta^{15}N$ of NO_3^- at all stations (Knapp et al., in prep). This depth horizon is also below the depth of the mixed layer at all stations, thus w_H is likely an upper limit if upwelling velocity decreases with depth. We also present the same calculations across the depth of the DCM for comparison.

Diffusive flux (J_{diff}; mmol m^{-2} d^{-1}) can also be calculated with knowledge of the concentration gradient below the base of the euphotic zone (mmol m^{-4}) and the vertical eddy diffusivity (m^2 d^{-1}):

$$J_{diff} = -K_z * \frac{\partial C_N}{\partial z}. \tag{11}$$

In this study, the gradient 10 m below the DCM was used for this calculation (and directly below the DCM). At Stations 1, 7, and 11.1, this depth horizon was within the depths sampled for ^7Be (80 m, 70 m, and 60 m, respectively). This horizon at Station 5 was at 140 m and at Station 11, 90 m; 60 m and 20 m deeper than ^7Be was measured, respectively. In these two cases, K_z is possibly an overestimate if the rate of eddy diffusivity decreases with depth.

Si and NO_3^- fluxes across the base of the euphotic zone were calculated at each station using the w_H and K_z values from Method A (Table 4). The columns presenting the advective flux of NO_3^- and Si are defined as the difference between the vertical flux into the surface box via upwelling and the horizontal export at the surface. Estimates for 11 and 11.1 are shown in parentheses to signify they most likely overestimate true fluxes and thus, these two stations will be ignored in further comparisons.

In most of the oligotrophic ocean, NO_3^- is the limiting nutrient, thus surface concentrations are near-zero. Our cruise track passed through regions where surface ocean NO_3^- concentrations were below detection

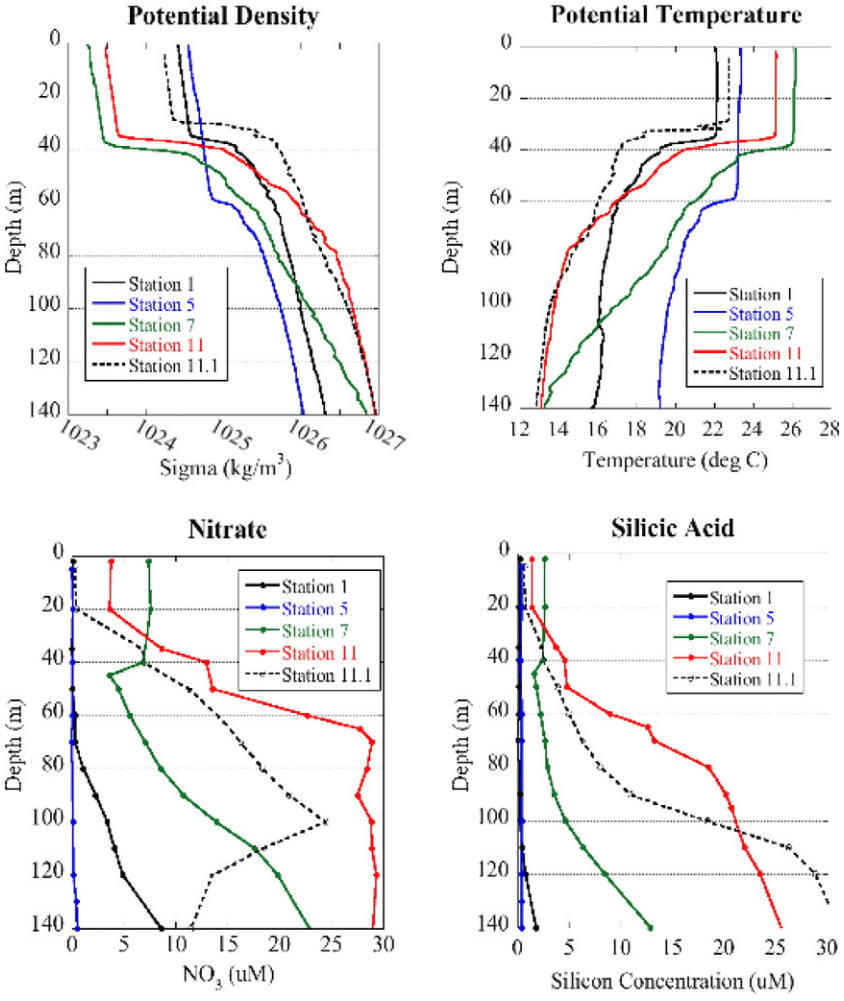

Fig. 5. Water column profiles of density, temperature, nitrate and silicic acid.

Table 4
Nutrient input fluxes 10 m below the DCM (all in mmol m^{-2} d^{-1}).

4a. Si Fluxes[a]

Station	Diffusive	Advective[b]	Total[c]	bSi Export[d]
1	0.03	0.02	0.05	0.05
5	0.02	0.0	0.02	0.06
7	0.66	0.08	0.73	0.50
11	1.9	56	(58)	0.05
11.1	2.5	2.5	(5)	–

4b. NO_3 fluxes[e]

Station	Diffusive	Advective	Total
1	0.52	0.33	0.85
5	0.15	0.0	0.15
7	3.3	−0.33	2.9
11	2.9	65	(68)
11.1	4.3	8.0	(12)

[a] ^{7}Be-based Si influx.
[b] Calculated as the vertical flux from upwelling minus the loss from the euphotic zone from horizontal advection.
[c] The sum of diffusive and advective fluxes.
[d] Th-based bSi export at 100 m calculated with 100 m trap Si:Th ratios.
[e] Calculated based on ^{7}Be; [NO_3] from Knapp et al., in prep.

(20°S stations) and where surface concentrations of NO_3^- were ~5 to 10 μM (10°S stations), signifying that NO_3^- was probably not always the limiting nutrient. The new production estimates presented in Table 5 are reported in mmol C m^- d^{-1}, calculated by multiplying the NO_3^- flux by a C:N ratio of 6.6. Also shown in Table 5 is Gross Primary Production (GPP), defined as total photosynthetic production, including that which is consumed by autotrophic respiration. GPP equals the ^{14}C-incubation primary production (Capone et al., in prep) integrated over the entire euphotic zone multiplied by the GPP/Net Primary Production (NPP) ratio of 2.7, a factor determined in multiple laboratory experiments of ^{14}C-incubation and ^{18}O–H_2O production studies run in parallel and confirmed in culture (Bender et al., 1987; Halsey et al., 2010; Marra, 2002). The rate of new production at Stations 1 and 5, where NO_3^- was completely consumed in the surface, was calculated to be 5.6 and 1.0 mmol C m^{-2} d^{-1}, respectively, which are 5% and 2% of the GPP at those stations. New production at Station 7 was 19 mmol C m^{-2} d^{-1}, which corresponds to 6% of the GPP.

New production calculated using the DCM as the euphotic depth horizon was approximately half the value of new production using the DCM + 10 m at Stations 1, 5 and 7 (Table 5). Although we believe that it is reasonable to assume the base of the euphotic zone is just below the DCM, this gives us an estimate of the amount of new nutrients which may be consumed within the chlorophyll maximum. Given that our estimate of the depth of the euphotic zone is uncertain, this exercise does provide an upper and lower limit to our calculated vertical nutrient fluxes. Both estimates fall within the range of independently determined export estimates at Stations 1 and 5, and the lower limit is within ±50% of export estimates at Station 7.

Table 5
Export fluxes and new production (all in mmol C m^{-2} d^{-1}).

	Stations				
Export	1	5	7	11	11.1
Traps[a]	0.8	0.4	1.2	0.6	1.3
DITD[b]	5.4	3.3	3.5	0.9	–
O_2 NCP[c] ^{7}Be-based	5.9	1.4	5.8	–	5.2
'New Prod' (DCM)[d]	3.4	0.6	9.0	(400)	(72)
'New Prod' (DCM + 10 m) Production	5.6	1.0	19	(449)	(81)
^{14}C PP[e]	44	22	111	160	90
GPP[f]	119	59	300	432	243
New Prod/GPP[g]	0.05	0.02	0.06	–	(0.33)

[a] Sediment traps set at 100 m (Haskell et al., 2013).
[b] Depth integrated thorium deficiency to 100 m (Haskell et al., 2013) multiplied by the C/^{234}Th ratio on trap material.
[c] Net community production in the mixed layer calculated from O_2/Ar measurements (Prokopenko et al., in prep).
[d] New production calculated from ^{7}Be-based total NO_3 flux across the deep Chl-a max (DCM) and DCM + 10 m; in C units (C:N = 6.6).
[e] Primary productivity integrated to 1% light (from Capone et al., in prep).
[f] Gross primary production calculated (^{14}C PP* 2.7; Marra, 2002).
[g] The ratio of 'New Prod' across the DCM-10 m horizon to GPP.

It is important to note, however, that at Station 7, the nitrate profile was anomalous in that the mixed layer concentration was significantly higher than the waters immediately below it (Fig. 5). This resulted in a negative net advective flux of nitrate to the surface because the concentration of surface waters exported horizontally was greater than that of the waters upwelled from below (Table 4). However, the net total nitrate flux is still positive since to the diffusive flux is an order of magnitude higher than the advective flux. One possible mechanism which could produce this nitrate profile could be a high rate of nitrate uptake by phytoplankton below the mixed layer producing either dissolved organic matter (DOM) or very small particles, which were then transported vertically into the mixed layer by mixing, entrainment or upwelling. There, they could subsequently be degraded into dissolved nitrate, with photodegredation being a possible mechanism. An alternative explanation is that the nitrate in the surface layer was transported horizontally from either within the ETSP or the equatorial upwelling to the north, which we ignore in our 1-dimensional model. Previous spatial nutrient surveys have shown that nitrate and phosphate accumulate between the Peru upwelling system and the equatorial upwelling system (centered at ~5°S, 105°W (Garcia et al., 2010)). Because of micronutrient limitation in this high-nutrient low-chlorophyll (HNLC) region, the horizontal flux from the two upwelling regions exceeds the loss to biological production. This 2-D view would suggest that horizontal transport of ^{7}Be could also lead to a downstream surface concentration gradient in ^{7}Be. However, the surface ^{7}Be concentration at Station 7 was 164 dpm m^{-3}, second smallest only to Station 11 (86 dpm m^{-3}) and ~half of the concentration at Station 1. This does not indicate that there is not a gradient in ^{7}Be, but instead that our data set is unable to resolve the downstream horizontal ^{7}Be gradient. Since the mean flow path is toward the northwest, no two stations fall on the same mean streamline (Fig. 1), and the expected patchiness of upwelling (Section 3.2) might further obscure a downstream signal.

3.5. Export flux: comparison of ^{7}Be-based estimates to other methods

In a steady-state system, new production should be balanced by export production (Eppley and Peterson, 1979). Here, we compare estimates of new production, based on ^{7}Be-derived transport parameters, to three independent metrics of export production: 1.) sinking flux estimates determined with floating sediment traps, 2.) Si/^{234}Th and C/^{234}Th ratios on trap material coupled with a water column ^{234}Th budget and, 3.) mixed layer O_2/Ar-derived Net Community Production (NCP). All three methods give a range of carbon flux estimates (Table 5). Different export estimates result from assumptions inherent to each method, which are discussed in Haskell et al. (2013) and Prokopenko et al. (in prep). Haskell et al. (2013) concluded that the sediment trap fluxes were most likely an underestimate as they systematically undercollected ^{234}Th. The Depth Integrated Thorium Deficiency (DITD) calculated fluxes appear to be more accurate, and are comparable to the oxygen-based estimates.

Si export estimated using the DITD and the Si:Th ratio measured in sediment traps set at 100 m is presented in Table 4. Because there is no dissolved organic form of Si and its only significant source to the surface ocean in the SE Pacific should be from below, the particulate export of Si should be balanced by the vertical flux from depth. Si export agrees with the ^{7}Be-calculated flux at Station 1 and is within a factor 1.5 to 3 at Stations 7 and 5, respectively.

The ^{7}Be-based new production estimates for carbon at Stations 1 and 5 are comparable to those based on traps, DITD and O_2/Ar (Table 5). This suggests that these regions were in steady-state at the time of sampling and that the calculated upwelling velocities and eddy diffusivities are reasonable estimates. Assuming that the DITD and O_2/Ar estimates of export are correct (~1–3× larger than the ^{7}Be-based new production), there may be additional sources of nutrients fueling particulate export at these stations, potentially including atmospheric deposition and/or nitrogen fixation (e.g. Deutsch et al., 2007; Westberry et al., 2006). However, based on the imperfect agreement observed for Si, we are unable to use this difference to quantitatively constrain any additional sources of fixed nitrogen. It is interesting to note that a complementary study based on water column δ^{15}N budgets suggests that nitrogen fixation may contribute up to 20% of the export production at Stations 1 and 5 (Knapp et al., in prep). At Station 7, the ^{7}Be-based new production estimates are ~3 times the estimate of export production based on O_2/Ar and ~5 times the value estimated from the DITD.

At Station 7, the Si balance for DITD and ^{7}Be only differ by a factor of 1.5, suggesting w_H and K_z may be reasonable (Table 4). However, the carbon fluxes predicted from ^{7}Be are 3 to 6 times greater than DITD depending on the choice of depth horizon. Part of this discrepancy might be attributed to both lateral and downward transport of DOM. The vertical nutrient fluxes would then be a better estimate of export production than particulate carbon flux. Haskell et al. (2013) used trap composition to conclude that these stations may support the highest export flux because the phytoplankton community is dominated by large species with sinking silica and carbonate tests, but did not address DOM. If the nutrient fluxes calculated here are correct, then DOM may play an important role in nutrient export.

3.6. Particle scavenging, evidence of non-steady state, and 2-D dynamics

At Stations 11 (10°S, 82°W) and 11.1 (15°S, 81°W), the deepest ^{7}Be samples were in excess of the activity of shallower samples (Fig. 4; Table 1). One mechanism that might produce this signal is particle scavenging in the surface and remineralization at depth. ^{7}Be is particle reactive; however we believe that particle scavenging can be ruled out as a possible source of this signal. Previous studies in the open ocean have shown that <10% of the ^{7}Be inventory is lost to particles (Aaboe et al., 1981; Andrews et al., 2008; Kadko and Johns, 2011; Kadko and Prospero, 2011; Silker, 1972a). At our stations, the fraction of ^{234}Th lost to particles was on average ~20% (Haskell et al., 2013). If this is characterized by a first order rate constant (k_p), then $k_p / (k_p + \lambda_{Th}) = 0.2$ and $k_p = 0.25 * \lambda_{Th}$. Bloom and Crecelius (1983), Nyffeler et al. (1984), Li et al. (1984), and Honeyman and Santschi (1988) have reported that the partition coefficient (K_d) of Th (~10^6 L kg^{-1}) is approximately an order of magnitude greater than that for Be (~10^5 L kg^{-1}). Thus, k_p' for ^{7}Be should be ~10% of k_p and the loss fraction of ^{7}Be by particle export should be: $k_p'/(\lambda_{Be} + k_p') = 0.025 * \lambda_{Th} / (\lambda_{Be} + 0.025 * \lambda_{Th})$, or ~5%. Therefore, this is unlikely to be a major sink for ^{7}Be in this study. It would be unlikely if the small amount of particulate ^{7}Be removed from the surface waters was remineralized in the narrow zone where we sampled, causing the deep maxima seen at Stations 11 and 11.1.

A second possible effect could be lateral transport. Haskell et al. (2013) argued that lateral advection was not a major ^{234}Th transport process at Station 11. However, ^{7}Be has a longer half-life and is potentially more susceptible to horizontal effects. Stations 11 and 11.1 had the highest lateral velocities in the study area (~5–10 cm s^{-1}); as shown by the calculation in Section 3.2, ^{7}Be can travel ~3–7° over its mean lifetime of ~80 days at this velocity. However, it seems unlikely that the high ^{7}Be activity sampled at ~80 m could be a transported signal. The maxima observed are in water at ~16 °C. Surface water this cold is not found until a latitude of 40–45°S, ~4.5 half-lives away. This water would need ~1500 dpm m^{-3} when it was subducted to arrive with the measured activity of ~100 dpm m^{-3} at 15°S. This is not an impossibly high concentration (given precipitation at this latitude in Fig. 1; Silker, 1972b), but it would need to travel undiluted and escape detection at Station 1 (Fig. 1; SE of 11 and 11.1). We believe this scenario is unlikely. High rainfall to the north is also a possible source for high ^{7}Be activity. However, given that there is no evidence in temperature or salinity for a surface water mass sourced from the north and subducted to 80 m, we cannot explain the anomalous ^{7}Be measurements with 2-D processes.

A third possible complication could be non-steady state. Using continuous measurement of O_2/Ar saturation in the mixed layer via an Equilibrator Inlet Mass Spectrometer (EIMS), Prokopenko et al. (in prep.) determined that during the 30 h of Station 11 occupation, the steady-state assumption was likely violated, as O_2/Ar was initially undersaturated by approximately −1%, but increased to 1.5% supersaturation, coincident with a sea-surface warming of approximately 1 °C. Also, CTD sampling throughout this period revealed rapid changes in the upper 100 m of the water column in salinity, temperature, O_2 saturation, as well as in the depth of the mixed layer (from 35 m to 16 m to 20 m; Prokopenko et al., in prep). Non-steady state processes may have contributed to the anomalous ^{7}Be profiles, particularly at Station 11, since all samples were not collected simultaneously. We believe this is the most likely cause, although cannot fully clarify its details.

4. Conclusions

We have presented water column upwelling velocities and eddy diffusivities from the ETSP using a seldom-utilized technique involving mass balances and vertical profiles for the cosmogenic isotope ^{7}Be. This method, along with measured nutrient distributions and particulate export, was used to estimate nutrient fluxes in the surface ocean between 10°S and 20°S in the Southeast Pacific. The upwelling rate at the eastern station that fits our 1-D geochemical model was 0.3 m d^{-1}, while the rates at stations further west, closer to the central gyre, ranged from 0.0 to 1.1 m d^{-1}, which are similar to previously published rates using other methods. The corresponding eddy diffusivities (K_z) calculated using our model at each station ranged from 0.43 to an upper limit of 2.6 cm^2 s^{-1}, which are also comparable to previous results, but larger than Yeung et al. (in review).

Applying these transport rates to nutrient distributions in the water column, vertical nutrient fluxes showed a clear difference between the 10°S and 20°S transects. ^{7}Be-based NO_3^- fluxes across the base of euphotic zone were 0.85 and 0.15 mmol m^{-2} d^{-1} at Stations 1 and 5 (20°S), respectively. At a station along the 10°S parallel (Station 7), we calculate a flux of 2.9 mmol m^{-2} d^{-1} of NO_3^- across the base of the euphotic zone. Each station along the southernmost transect (20°S) had surface ocean NO_3^- concentrations at or below detection limits, and the ^{7}Be-based new production calculated from nutrient fluxes at each station fell within the range of export production estimated with sediment traps, ^{234}Th/^{238}U disequilibrium, and mixed layer O_2/Ar ratios (1.0 to 5.6 mmol m^{-2} d^{-1}). At Station 7, NO_3^- concentrations in the surface waters were >7 μM and the ^{7}Be-based nutrient fluxes exceeded export production by a factor of 3 (19 mmol m^{-2} d^{-1}). We interpret the difference between ^{7}Be and other export metrics at Station 7 as possibly the result of high DOM production and its downward vertical export or lateral surface transport. Two stations to the east also had relatively high surface NO_3^-, but showed evidence of non steady-state behavior and appeared to provide upper limits for nutrient fluxes (Stations 11 and 11.1).

Ignoring these two stations, we estimate that the amount of new production that can be supported from new nutrients transported vertically from below range from 1.0 to 19 mmol C m^{-2} d^{-1} over the entire study region. The new production estimates corresponded to NCP/GPP ratios ranging from 0.02 to 0.06, consistent with the expectation for low export efficiency in ecosystems that are more nutrient limited compared to ecosystems with a higher nutrient supply. Rates of new production at Stations 1 and 5 calculated using the ^{7}Be-based method fell below the upper limit of export estimates, suggesting another source of nutrients may be contributing to export production,

potentially including nitrogen fixation in the surface waters at these nitrate-limited stations.

Acknowledgments

We would like to first thank the captain and crew of the *R/V Melville* for their invaluable help during the cruise. Special thanks to Troy Gunderson and Nick Rollins for all the hard work making the ETSP cruises run as smoothly as they did. Thanks to Rick Schwartz (USC), Christa Wolfe (USC) and Mark Stephens (RSMAS) for Si, bSi and ^{7}Be analysis respectively. Thanks to Matt Tiahlo for performing the ^{14}C primary productivity experiments. We would also like to thank M. Rutgers van der Loeff, P. Santschi and an anonymous reviewer for their helpful comments and suggestions. Funding was provided by NSF Chemical Oceanography grants OCE0850801 to William Berelson, Angela Knapp and Douglas Capone, OCE0961207 to Douglas Hammond and William Berelson, and OCE1034746 to David Kadko.

References

Aaboe, E., Dion, E.P., Turekian, K.K., 1981. Be-7 in Sargasso Sea and Long Island Sound Waters. J. Geophys. Res. Oceans Atmos. 86 (NC4), 3255–3257.
Aldahan, A., Possner, G., Vintersved, I., 2001. Atmospheric interactions at northern high latitudes from weekly Be-isotopes in surface air. Appl. Radiat. Isot. 54 (2), 345–353.
Anderson, J.J., 1978. Deep ocean mining and the ecology of the tropical North Pacific. Univ. of Washington, Seattle, WA.
Andrews, J.E., Hartin, C., Buesseler, K.O., 2008. ^{7}Be analyses in seawater by low background gamma-spectroscopy. J. Radioanal. Nucl. Chem. 277 (1), 253–259.
Bender, M., Grande, K., Johnson, K., Marra, J., Williams, P.J.L., Sieburth, J., Pilson, M., Langdon, C., Hitchcock, G., Orchardo, J., Hunt, C., Donaghay, P., Heinemann, K., 1987. A comparison of 4 methods for determining planktonic community production. Limnol. Oceanogr. 32, 1085–1098.
Bloom, N., Crecelius, E.A., 1983. Solubility behavior of atmospheric ^{7}Be in the marine environment. Mar. Chem. 12, 323–331.
Braman, R.S., Hendrix, S.A., 1989. Nanogram nitrate determination in environmental and biological materials by vanadium (III) reduction with chemiluminescence detection. Anal. Chem. 61 (24), 2715–2718.
Broecker, W.S., Peng, T.-H., 1982. Tracers in the sea. Eldigio Press, Palisades, New York U.S.A. (690 pp.).
Broecker, W.S., Peng, T.H., Stuiver, M., 1978. An estimate of the upwelling rate in the Equatorial Atlantic based on the distribution of bomb radiocarbon. J. Geophys. Res. 83, 6179–6186.
Capone, D.G., Tiahlo, M., Gunderson, T.E., Knapp, A.N., Berelson, W.M., 2014n. Patterns of primary production in surface waters along two offshore transects in the Eastern Tropical South Pacific, (in preparation).
Deutsch, C., Sarmiento, J.L., Sigman, D.M., Gruber, N., Dunne, J.P., 2007. Spatial coupling of nitrogen inputs and losses in the ocean. Nature 445, 163–167.
Dugdale, R.C., Goering, J.J., 1967. Uptake of new and regenerated forms of nitrogen in primary productivity. Limnol. Oceanogr. 12 (2), 196–206.
Eppley, R.W., Peterson, B.J., 1979. Particulate organic matter flux and planktonic new production in the deep ocean. Nature 282, 677–680.
Feely, H.W., Larsen, R.J., Sanderson, C.G., 1989. Factors that cause seasonal variations in Beryllium-7 concentrations in surface air. J. Environ. Radioact. 9 (3), 223–249.
Forbush, Scott E., 1954. World-wide cosmic ray variations, 1937–1952. J. Geophys. Res. 59 (4), 525–542.
Garcia, H.E., Locarnini, R.A., Boyer, T.P., Antonov, J.I., Zweng, M.M., Baranova, O.K., Johnson, D.R., 2010. World Ocean Atlas 2009, Volume 4: nutrients (phosphate, nitrate, silicate). In: Levitus, S. (Ed.), NOAA Atlas NESDIS 71. U.S. Government Printing Office, Washington, D.C., p. 398.
Gnanadesikan, A., Dunne, J.P., Key, R.M., Matsumoto, K., Sarmiento, J.L., Slater, R.D., Swathi, P.S., 2004. Oceanic ventilation and biogeochemical cycling: understanding the physical mechanisms that produce realistic distributions of tracers and productivity. Glob. Biogeochem. Cycles 18, 4.
Halsey, K.H., Milligan, A.J., Behrenfeld, M.J., 2010. Physiological optimization underlies growth rate-independent chlorophyll-specific gross and net primary production. Photosynth. Res. 103, 125–137.
Harrison, D.E., 1996. Vertical velocity in the central tropical Pacific: a circulation model perspective for JGOFS. Deep Sea Res. II 43, 687–705.
Haskell, W.Z.II., Berelson, W.M., Hammond, D.E., Capone, D.G., 2013. Particle sinking dynamics and POC fluxes in the Eastern Tropical South Pacific based on ^{234}Th budgets and sediment trap deployments. Deep-Sea Res. I 81, 1–13.
Hayes, S.P., Chang, P., McPhaden, M.J., 1991. Variability of the sea surface temperature in the Eastern Equatorial Pacific during 1986–1988. J. Geophys. Res. 96, 10553–10556.
Honeyman, B.D., Santschi, P.H., 1988. Metals in aquatic systems. Environ. Sci. Technol. 22, 862–871.
Kadko, D., 2000. Modeling the evolution of the arctic mixed layer during the fall of 1997 SHEBA project using measurements of ^{7}Be. J. Geophys. Res. 105, 3369–3378.
Kadko, D., 2009. Rapid oxygen utilization in the ocean twilight zone assessed with the cosmogenic isotope ^{7}Be. Glob. Biogeochem. Cycles 23. http://dx.doi.org/10.1029/2009GB003510 GB4010.
Kadko, D., Johns, W., 2011. Inferring upwelling rates in the equatorial Atlantic using ^{7}Be measurements in the upper ocean. Deep-Sea Res. I 58, 647–657.
Kadko, D., Johnson, R., 2008. Insights into 18 degree mode water formation from measurements of ^{7}Be at the Bermuda Time-Series station. Ocean Sci. Meet. Suppl. Abstr.
Kadko, D., Olson, D., 1996. Beryllium-7 as a tracer of surface water subduction and mixed-layer history. Deep-Sea Res. I 43 (2), 89–116.
Kadko, D., Prospero, J., 2011. Deposition of ^{7}Be to Bermuda and the regional ocean: environmental factors affecting estimates of atmospheric flux to the ocean. J. Geophys. Res. 116. http://dx.doi.org/10.1029/2010JC006629 C02013.
Kadko, D., Swart, P., 2004. The source of the high heat and freshwater content of the upper ocean at the SHEBA site in the Beaufort Sea in 1997. J. Geophys. Res. 109. http://dx.doi.org/10.1029/2002JC001734 (C01022).
Karl, David M., et al., 1992. Trichodesmium blooms and new nitrogen in the North Pacific gyre. Marine pelagic cyanobacteria: Trichodesmium and other diazotrophs. Springer, Netherlands, pp. 219–237.
Klein, B., Rhein, M., 2004. Equatorial upwelling rates inferred from helium isotope data: a novel approach. Geophys. Res. Lett. 31. http://dx.doi.org/10.1029/2004GL021262 L23308.
Knapp, A.N., Casciotti, K.L., Berelson, W.M., Prokopenko, M.G., Capone, D.G., 2014n. Low rates of nitrogen fixation in Eastern Tropical South Pacific surface waters, in preparation.
Krishnaswami, S., Lal, D., Somayajulu, B.L.K., Dixon, F.S., Stonecipher, S.A., Craig, H., 1972. Silicon, radium, thorium and lead in seawater: in-situ extraction by synthetic fibre. Earth Planet. Sci. Lett. 16, 84–90.
Lal, D., Chung, Y., Platt, T., Lee, T., 1988. Twin cosmogenic radiotracer studies of phosphorus recycling and chemical fluxes in the upper ocean. Limnol. Oceanogr. 336, 1559–1567.
Lee, T., Barg, E., Lal, D., 1991. Studies of vertical mixing in the Southern California Bight with cosmogenic radionuclides ^{32}P and ^{7}Be. Limnol. Oceanogr. 365, 1044–1053.
Leppänen, A.-P., et al., 2010. Cosmogenic ^{7}Be in air: a complex mixture of production and transport. J. Atmos. Solar-Terr. Phys. 72 (13), 1036–1043.
Li, Y.H., Burkhardt, L., Buchholtz, M., O'Hara, P., Santschi, P.H., 1984. Partition of radiotracers between suspended particles and seawater. Geochim. Cosmochim. Acta 48 (10), 2011–2019.
Approaches to measurements of plankton production. In: Marra, J. (Ed.), Phytoplankton Productivity and Carbon Assimilation in Marine and Freshwater Ecoystems. Blackwell, London.
Nagai, H., Tada, W., Kobayashi, T., 2000. Production rates of ^{7}Be and ^{10}Be in the atmosphere. Nucl. Inst. Methods Phys. Res. B 172, 796–801.
NASA Tropical Rainfall Measuring Mission (TRMM), 2014. National Aeronautics and Space Administration. http://trmm.gsfc.nasa.gov/ Web. Mar. 04.
NOAA Live Access Server, 2011. NOAA Ocean Watch-Central Pacific. National Oceanographic and Atmospheric Administration. http://oceanwatch.pifsc.noaa.gov/las/servlets/dataset (Web. Nov 15).
Nyffeler, U.P., Li, Y., Santschi, P.H., 1984. A kinetic approach to describe trace-element distribution between particles and solution in natural aquatic systems. Geochim. Cosmochim. Acta 48, 1513–1522.
Parsons, T.R., Maita, Y., Lalli, C.M., 1984. A manual of chemical and biological methods for seawater analysis. Pergamon, New York 173 pp.
Platt, T., Lewis, R., Geider, R., 1984. Thermodynamics of the pelagic ecosystems: elementary closure conditions for biological production in the open ocean. Flows of energy and materials in marine ecosystemsNATO Conference Series 13, pp. 49–84.
Prokopenko, M.G., Hammond, D.E., Berelson, W.M., Yeung, L.Y., Haskell, W.Z.II., Knapp, A.N., Stanley, R.H.R., Rollins, N., Yound, E.D., Capone, D.G., 2014. Net community and gross primary production and carbon export in the transition zone between the Peru Current and South Pacific Gyre, as determined with dissolved O_2/Ar ratios and oxygen triple isotope composition of O_2, (in prepartion).
Quay, P.D., Stuiver, M., Broecker, W.S., 1983. Upwelling rates for the equatorial Pacific Ocean derived from the bomb ^{14}C distribution. J. Mar. Res. 41, 769–792.
Reiter, E.R., 1978. Atmospheric transport processes. Part 4. Radioactive tracers. U.S. DOE. NTIS TID27114.
Rhein, M., Dengler, M., Sültenfuß, J., Hummels, R., Hüttl-Kabus, S., Bourles, B., 2010. Upwelling and associated heat flux in the equatorial Atlantic inferred from helium isotope disequilibrium. J. Geophys. Res. 115. http://dx.doi.org/10.1029/2009C005772 C08021.
Rutgers van der Loeff, M.M., Moore, W.S., 1999. Determination of natural radioactive tracers. Methods of Seawater Analysis. Verlag Chemie, Weinheim (Ch. 13).
Schlitzer, R., 2014. Ocean Data View. http://www.odv.awi.de.
Silker, W.B., 1972a. Horizontal and vertical distributions of radionuclides in the North Pacific Ocean. J. Geophys. Res. 77 (6), 1061–1070.
Silker, W.B., 1972b. Beryllium-7 and fission products in the GEOSECS II water column and applications of their oceanic distributions. Earth Planet. Sci. Lett. 16, 131–137.
Strickland, J.H., Parsons, T.R., 1968. A practical handbook of seawater analysis. Fish. Res. Board Can. Bull. 167, 71–75.
Swenson, M.S., Hansen, D.V., 1999. Tropical Pacific ocean mixed layer heat budget: the Pacific cold tongue. J. Phys. Oceanogr. 29, 69–81.
Toggweiler, J.R., Dixon, K., Broecker, W.S., 1991. The Peru upwelling and the ventilation of the South Pacific thermocline. J. Geophys. Res. Oceans 96 (C11), 20467–20497 (1978–2012).
Vainio, R., Desorgher, L., Heynderickx, D., Storini, M., Fluckiger, E., Horne, R.B., Kovaltsov, G.A., Kudela, K., Laurenza, M., McKenna-Lawlor, S., Rothkaehl, H., Usoskin, I.G., 2009. Dynamics of the Earth's particle radiation environment. Space Sci. Rev. 147 (3–4), 187–231.
Wanninkhof, R., Feely, R.A., Atwood, D.K., Berberian, G., Wilson, D., Murphy, P.P., Lamb, M.F., 1995. Seasonal and lateral variations in carbon chemistry of surface water in the eastern equatorial Pacific during 1992. Deep-Sea Res. II 42, 387–409.

Westberry, T.K., Siegel, D.A., 2006. Spatial and temporal distribution of Trichodesmium blooms in the world's oceans. Glob. Biogeochem. Cycles 20. http://dx.doi.org/10.1029/2005GB002673 GB4016.
Word Ocean Atlas, 2009. National Oceanographic Data Center. U.S. Dept. of Commerce. http://www.nodc.noaa.gov/OC5/WOA09/pr_woa09.html (Accessed 2014).
Wyrtki, K., 1963. The horizontal and vertical field of motion in the Peru Current. University of California Press.
Wyrtki, K., 1981. An estimate of equatorial upwelling in the Pacific. J. Phys. Oceanogr. 11, 1205–1214.
Yeung, L.Y., Berelson, W.M., Hammond, D.E., Prokopenko, M.G., Wolfe, C., Rollins, N., 2014w. Upper-ocean gas dynamics for biogeochemical applications using radon profiles in the Eastern Tropical South Pacific. Deep-Sea Res. I in review.
Young, J.A., Silker, W.B., 1980. Aerosol deposition velocities on the Pacific and Atlantic oceans calculated from ^{7}Be measurements. Earth Planet. Sci. Lett. 50 (1), 92–104.